Recent tectonic activity of Iran deduced from young magmatism evidences

Jamshid AHMADIAN, Mamoru MURATA, Alireza NADIMI
Hiroaki OZAWA and Takeshi KOZAI

鳴門教育大学学校教育研究紀要

第28号

Bulletin of Center for Collaboration in Community
Naruto University of Education
No.28, Feb., 2014

原 著 論 文

鳴門教育大学学校教育研究紀要　28，23 － 38

Recent tectonic activity of Iran deduced from young magmatism evidences

Jamshid AHMADIAN [a, b], Mamoru MURATA [c], Alireza NADIMI [d], Hiroaki OZAWA [e] and Takeshi KOZAI [c]

[a] Department of Geology, Payame Noor University, P.O. Box 19395-3697, Tehran, IRAN
[b] Center for collaboration in community, Naruto University of Education, Naruto, Tokushima, 772-8502, Japan
[c] Natural Science Education (Science), Naruto University of Education, Naruto, Tokushima, 772-8502, Japan
[d] Department of Geology, Faculty of Science, University of Isfahan, P.O. Box 81746-73441, Isfahan, Iran
[e] International Cooperation Center for the Teacher Education and Training, Naruto, Tokushima, 772-8502, Japan

Abstract：Closure of the Neo-Tethys Ocean during Mesozoic and Cenozoic is one of the most important stages of tectonic evolution of Iranian Plateau. Subduction of the oceanic lithosphere under the southwestern border of Central Iran, caused plutonic and volcanic activity between the Jurassic and Quaternary within and adjacent to the southern margin of Central Iran. During closure of the ocean, two major subduction-related arcs trending parallel to the Main Zagros Thrust, the Mesozoic Sanandaj-Sirjan (SSMA) and the Tertiary to Plio-Quaternary Urumieh-Dokhtar magmatic arcs (UDMA) have been formed. Quaternary volcanic activity, generated by a complex combination of geodynamic and petrogenetic processes associated with the evolution of the Alpine-Himalayan collision belt. This volcanic activity has produced both andesitic stratovolcanoes and fields of basaltic cones and plateau lavas. Upper Miocene to Pliocene-Quaternary volcanic activity is observable in Makran, UDMA, Qom-Baft, Anar and northern Lut.

Keywords：Active Tectonics, Magmatism, Quaternary volcanism, UDMA, Central Iran, Iran.

Ⅰ. Introduction

The tectonic evolution of Iran involves several deformation stages (Berberian and Berberian, 1981). One of the most important stages is tectonic evolution of the Neo-Tethys Ocean after Permian and its closure in Cenozoic. Northward motion of Arabia in the late Mesozoic and early Cenozoic was associated with subduction under the southern margin of Eurasia.

The Zagros Orogen is a young, active and linear collisional orogen that is formed after closure of the Neo-Tethys Ocean and constitutes part of the Alpine-Himalayan orogenic belt (e.g. Stöcklin 1968; Ricou 1971; Dewey *et al*. 1973; Berberian and King 1981; Koop and Stoneley 1982; Ziegler and Stampfli 2001; Blanc *et al*. 2003). The age of initial collision is disputed, with suggested ages ranging from ~10-12 Ma (Late Miocene, Dewey *et al*., 1986; McQuarrie *et al*., 2003) to ~35-40 Ma (Middle-Late Eocene; Hempton, 1987; Hessami *et al*., 2001; Vincent *et al*., 2005). Early deformation and changing sedimentation patterns on both sides of the Arabia-Eurasia (Bitlis-Zagros) suture indicate a Late Eocene age (~35 Ma), consistent with a sharp reduction in magmatism between the Eocene and Oligocene (Allen and Armstrong, 2008).

Collision between the Arabian and Eurasian plates is active, shown by the complex seismicity of SW Asia, the GPS-derived velocity field and abundant evidence for neotectonic faulting in Iran, Turkey and adjacent countries (Jackson *et al*., 1995; Vernant *et al*., 2004). The Turkish-Iranian plateau is not undergoing major active crustal thickening (e.g. Berberian and Yeats, 1999), although earlier collision-generated thickening is indicated by both present Moho depths (commonly 45-60 km) and the record of mid Cenozoic compressional deformation (Allen *et al*., 2004). The plateau has typical elevations of 1.5-2 km, trailing off westwards in to western Turkey and eastwards in to the deserts of eastern Iran. Folding and thrusting are active at its margins, in ranges such as the Zagros and Alborz (Jackson *et al*., 1995), but far less so within the plateau interior. Active tectonics of NW Iran involve a counterclockwise rotating array of NW-SE trending, right-lateral strike-slip faults (Copley and Jackson, 2006).

The major tectonic zones of the Zagros orogenic belt (Fig. 1) recorded several deformation events since Cretaceous

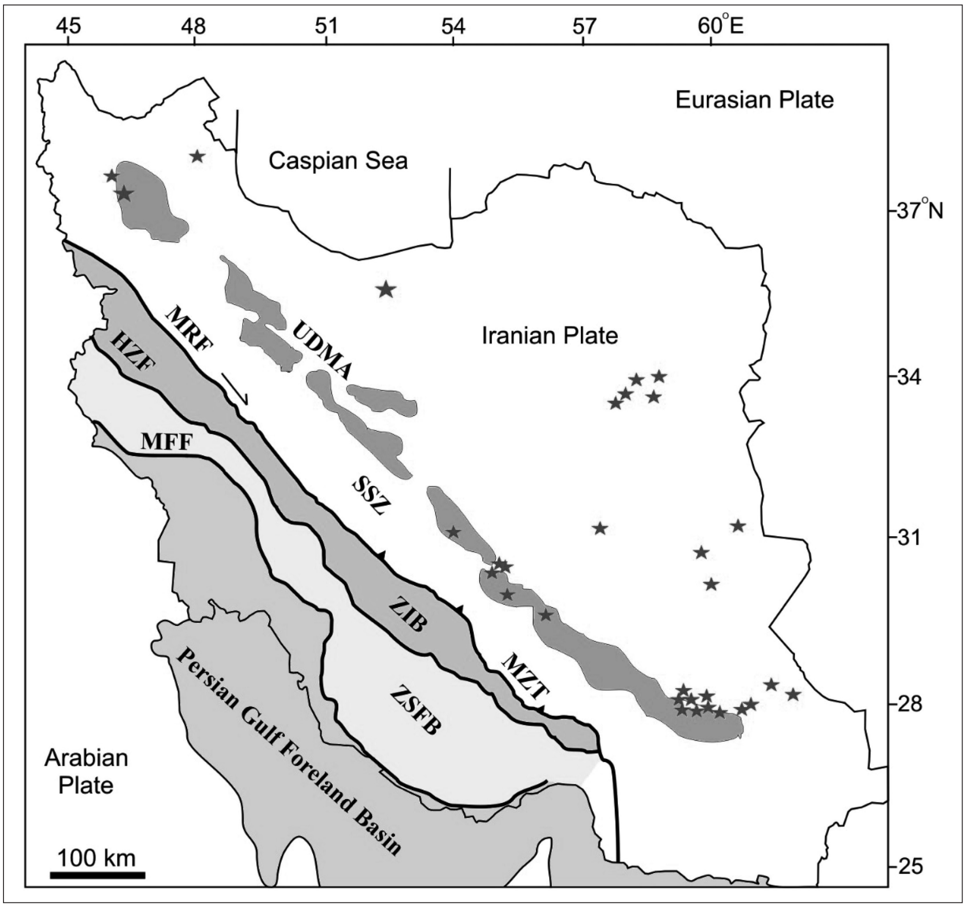

Figure 1. Tectonic zones of the Zagros Orogen: ZSFB- Zagros Simply Folded Belt, ZIB- Zagros Imbricate Belt (High Zagros Belt), SSZ- Sanandaj-Sirjan Zone, UDMA- Urumieh-Dokhtar Magmatic Arc.
Major faults: MFF- Mountain Front Fault, HZF- High Zagros Fault, MRF- Main Recent Fault and MZT- Main Zagros Thrust (Stöcklin 1968; Falcon 1974; Berberian and King 1981, Alavi 1994; Berberian 1995; Agard *et al*. 2005). Red stars mark Quaternary volcanoes with craters and calderas (based on Huber 1977).

times (Falcon 1969, 1974; Haynes and McQuillan 1974; Koop and Stoneley 1982; Alavi 1994; Berberian 1995; Agard *et al*. 2005). The Zagros Orogen is sub-divided into several tectonic units. Falcon (1969, 1974) sub-divided the Zagros Orogen into three zones: the Thrust Zone, the Imbricate Zone and the Simply Folded Zone. The main deformation zone according to Stöcklin (1968, 1974) is defined as the Main Zagros Thrust, which is the suture between the Arabian and Eurasian plates (Iranian Plate) and the northeast border of the Zagros Fold-Thrust Belt (Fig. 1).

Based on previous studies (e.g. Stöcklin 1968; Falcon 1974; Alavi 1994; Berberian and King 1981, Berberian 1995; Agard *et al*. 2005), the following sub-division of tectonic units in the Zagros Orogen, located north-eastwards of the Persian Gulf Foreland Basin will be applied in this research: the Zagros Simply Folded Belt, the Zagros Imbricate Belt, the Sanandaj-Sirjan Zone and the Urumieh-Dokhtar Magmatic Arc (Fig. 1).

The Urumieh-Dokhtar Magmatic Arc (UDMA) is an Andean-type volcanic magmatic arc (Schröder 1944), with an almost continuous calc-alkaline magmatic activity from the Eocene till present (e.g. Berberian and Berberian 1981; Berberian and King 1981; Bina *et al*. 1986), which peaked during the Oligocene-Miocene. This belt is one of the most important magmatic belts of Iran and adjacent areas that is formed during subducting of the Tethyan oceanic crust under the Central Iran.

The aim of this paper is review and describing the recent tectonic activity of Iran deduced from young magmatism evidences during Miocene-Quaternary. These magmatism activity usually started from Mesozoic and are continued until present.

Ⅱ. Geological settings

1. Outline

The collision of two continental plates produces a zone of very complex tectonic structures. Many kinds of such tectonic structures formed also during Cenozoic times in the Zagros Orogen and other parts of Iranian Plateau, as a consequence of the collision between the Arabian and the Eurasian plates (e.g., Stöcklin, 1968). Most of these structures are still active. Addition to young magmatism, tectonic deformation in Iran during the last 3-5 Ma resulted in the N-S-trending convergence, dextral strike-slip faulting (e.g., Berberian and King, 1981; Berberian, 1981) and partly in thrusting and accompanying folding.

2. Urumieh-Dokhtar Magmatic Belt

The Urumieh-Dokhtar Magmatic Arc (UDMA) forms a distinct linear, over 4 km thick intrusive- extrusive complex (Alavi 1994), which extends along the entire length of the Zagros Orogen (Fig. 1). The UDMA ranges in age from the Cretaceous till Recent, but is dominated by 50-35 Ma intermediate to acidic volcanic and plutonic rocks (Alavi 1980; Berberian and King 1981; Berberian *et al*. 1982). The UDMA comprises various lithological units including gabbros, diorites, granodiorites and granite bodies of different size (e.g. Haghipour and Aghanabati 1985). Basaltic lava flows, trachybasalts, ignimbrites and pyroclastic rocks, mostly tuffs and agglomerates, are also widely distributed in the unit (Alavi 1994).

Extrusive volcanism in the UDMA began in the Eocene and continued for the rest of this period, with a climax in the Middle Eocene (Berberian and King 1981). Geochemical studies indicate that the UDMA is composed of subduction-related calc-alkaline (e.g. Forster *et al*. 1972; Jung *et al*. 1976; Berberian *et al*. 1982), and calc-alkaline and tholeiitic rocks (e.g. Ahmad and Posht Kuhi 1993).

It is generally assumed that the UDMA was the magmatic arc overlying the slab of the Neo-Tethyan oceanic lithosphere, which was subducted beneath the Iranian Plate (Alavi 1980, 1994; Berberian and Berberian 1981). Amidi *et al*. (1984) proposed a rift model for the interpretation of the origin of Eocene volcanic rocks. Ghasemi and Talbot (2006) suggested a post-collision model for post-Middle Eocene igneous rocks of the UDMA. However, based on geochemical studies of igneous rocks from the Shahr Babak region (NW of Sirjan town), Hassanzadeh (1993) proposed a continental-arc setting.

This is supported by geochemical studies and isotope data from the Miocene Sar-Cheshmeh porphyry copper deposit that is located in the UDMA, indicating a primitive to mature island-arc setting for the deposit (Shahabpour and Kramers 1987; Shahabpour 2007). Other evidence are Eocene alkaline rocks of the south Rafsanjan region (Hassanzadeh 1993), Upper Eocene calk-alkaline volcanic rocks from the boundary of the Iranian Plate and the Rafsanjan basin (Nazari *et al*., 1994), and an increase in slab dip of the subducting Neo-Tethys oceanic crust during the Early Miocene (Berberian and Berberian 1981).

Magmatism in the UDMA occurred chiefly during the Eocene but later resumed, after a quiescent period, during the Upper Miocene to Plio-Quaternary. Age constraints for the UDMA volcanics are mostly inferred from their position with respect to fossil-bearing sedimentary units, except for a few isotopic ages (37.5 ± 1.4 to 2.8 ± 0.2 Ma in the Anar-Shahr Babak region; Hassanzadeh, 1993; 33-20 Ma for Natanz pluton; Berberian *et al*., 1982). Note that this Eocene magmatic activity in the UDMA is also coeval with a widespread magmatic activity throughout most of the Iranian plateau.

Ⅲ. Neo-Tethys and Tethyan oceans

Subduction of the Tethyan oceanic lithosphere under the southwestern border of Central Iran, caused plutonic and volcanic activity between the Jurassic and Quaternary within and adjacent to the southern margin of Central Iran (Fig. 1) (Ricou *et al*., 1977; Berberian and King, 1981; Berberian, 1983; Mohajjel *et al*., 2003). The tectonic history of the Tethyan region has been studied by many authors (e.g., Takin, 1972; Stocklin, 1974; Berberian, 1981; Berberian and King, 1981; Berberian and Berberian, 1981; Berberian *et al*., 1982; Sengor, 1984, 1990; Shahabpour and Kramers, 1987; Alavi, 1994; Nadimi 2002; Shahabpour, 2005; Torsvik and Cocks, 2013). Since Paleozoic time, Central Iran was part of the Gondwana, separated from the Laurasian plate by the Paleo-Tethys (Fig. 2).

The closure of Paleo-Tethys during Triassic time by northward motion of the Central Iran micro-continent resulted in its welding with the Eurasian plate (e.g., Shahabpour 2007). Sometime prior to the Middle Triassic, the Late Paleozoic ophiolites were emplaced in the north, presumably at the time of collision of continental fragments with the Laurasian plate.

About the same time during closure of the Paleo-Tethys in the north, rifting along the present Zagros thrust zone (Fig. 1) took place, resulting in opening of a new ocean called the

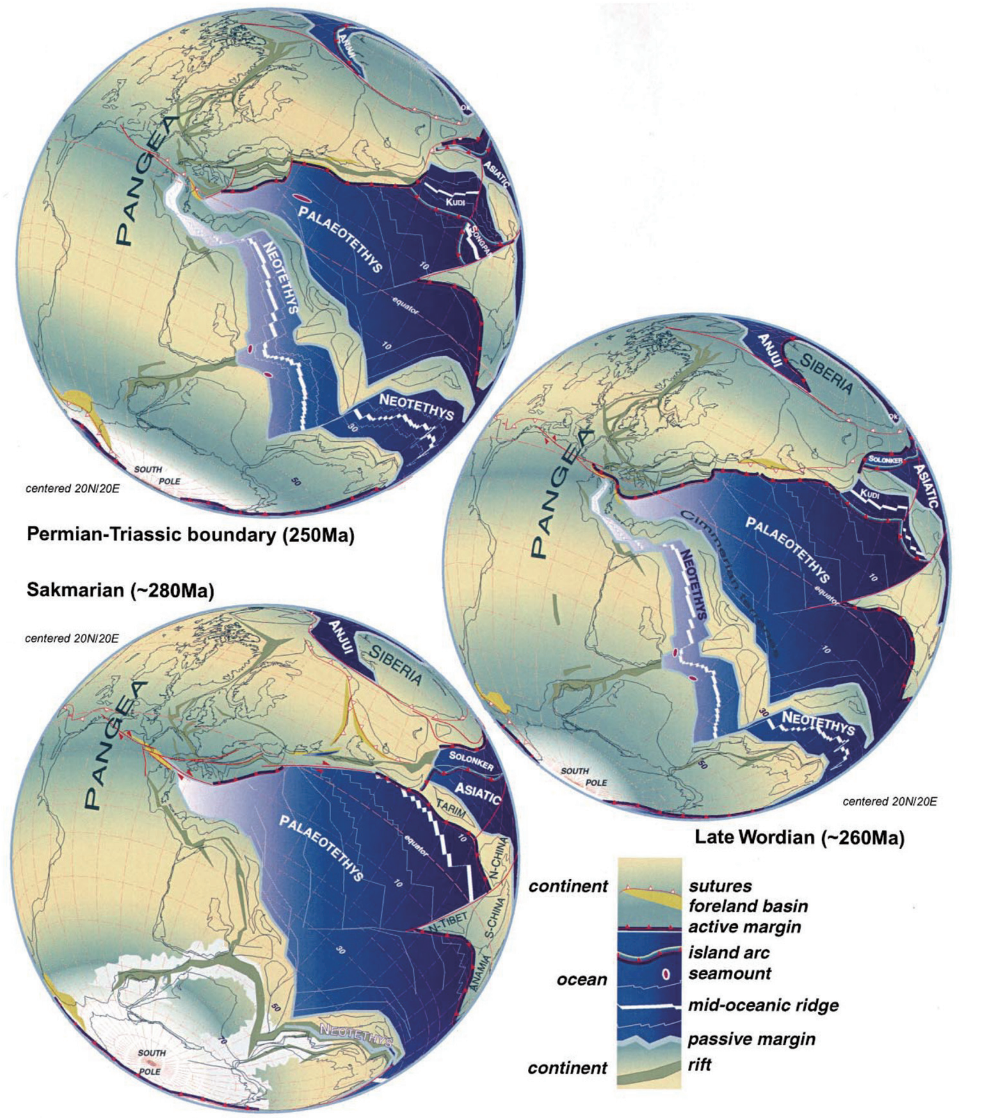

Figure 2. Reconstruction of Paleo-Tethys Ocean and adjacent continent. Orthographic projection with Europe fixed in its present-day position.
Paleopoles of Baltica are used as reference for the paleolatitudes (Stampfli and Borel, 2002).

Neo-Tethys. With disappearance of the Paleo-Tethys in the north, the floor of Neo-Tethys started to subduct beneath Central Iran during Triassic-Jurassic time (Fig. 3).

This led to an Early Cimmerian metamorphic event, recorded southwest of the Sanandaj-Sirjan zone (Berberian and King, 1981; Berberian and Berberian, 1981; Hooper *et al.*, 1994), and also Upper Triassic emplacement of intrusive bodies such as Siah Kuh granite batholith (Sabzehei, 1994; Berberian and Berberian, 1981) within this zone (Fig. 1). The final closure of Neo-Tethys and collision between Arabia and Central Iran took place during the Neogene (Berberian and Berberian, 1981; Berberian *et al.*, 1982).

Ⅳ. Magmatism in Iran

Implications for initiation of Neo-Tethys subduction It is generally believed that the detachment of Central Iran from Arabia during Late Permian and its northwestward movement led to the formation of a new ocean (Neo-Tethys) along the present main Zagros folded-thrust belt (Berberian and Berberian, 1981; Berberian and King, 1981). The Middle Triassic orogeny in Iran is interpreted as the result of subduction of the Neo-Tethys oceanic crust underneath Central Iran, which initiated regional metamorphism and magmatism along the Sanandaj-Sirjan zone (Berberian and King, 1981).

Little is known, however, about the long-lasting magmatic activity (150 m.y.) of the two presumably subduction-related

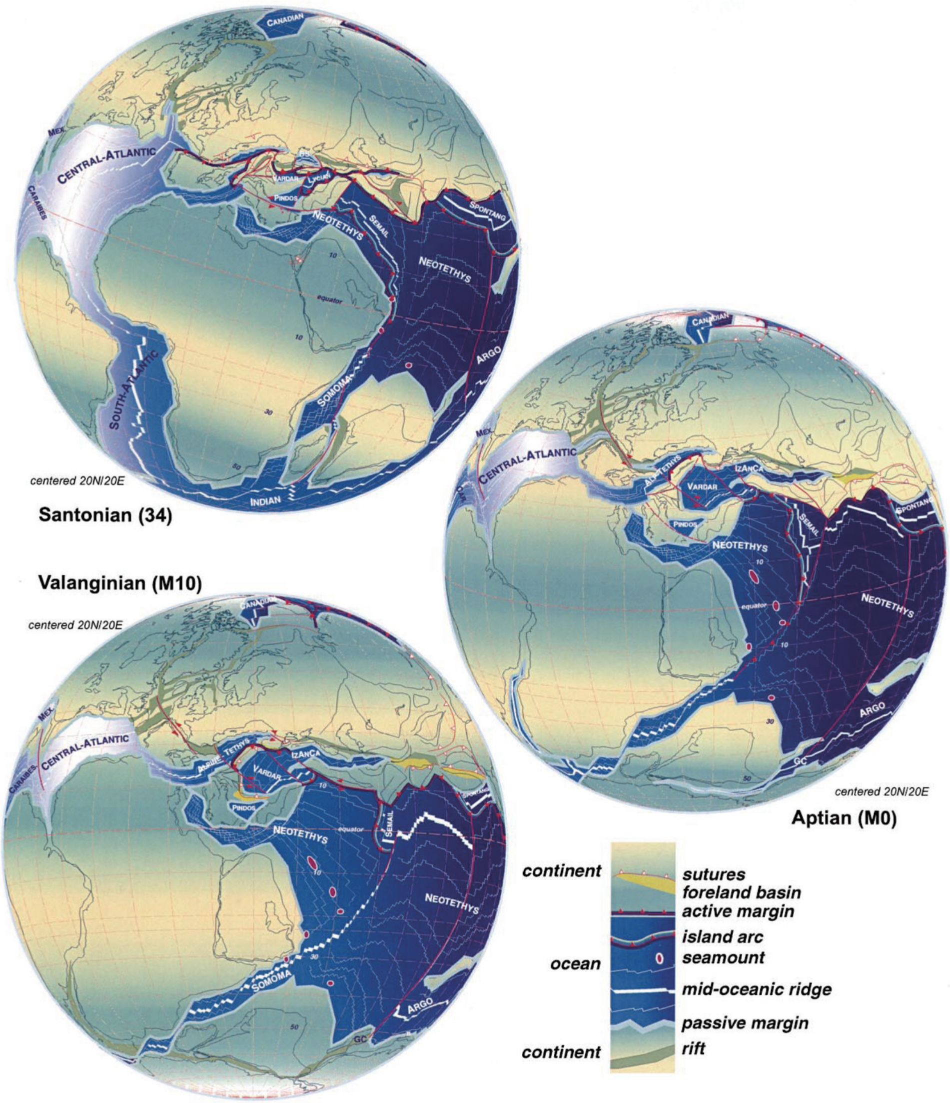

Figure 3. Reconstruction of Neo-Tethys Ocean and adjacent continent. Orthographic projection with Europe fixed in its present-day position. Paleopoles of Baltica are used as reference for the paleolatitudes (Stampfli and Borel, 2002).

arcs trending parallel to the Main Zagros Thrust, namely, the Mesozoic Sanandaj-Sirjan (SSMA) and the Tertiary to Plio-Quaternary Urumieh-Dokhtar magmatic arcs (UDMA) (Fig. 4). Despite abundant exposures of igneous rocks in both the SSMA and the UDMA (Fig. 4a), few studies are available (Berberian and Berberian, 1981; Berberian *et al.*, 1982; Shahabpour, 2005; Ahmadi Khalaji *et al.*, 2007) and no geochemical data have been acquired on a regional scale to better constrain the subduction history of Zagros. During this period, plutonic activity was episodic, probably due to episodic plate motions and changes in the consumption rate of the oceanic crust, with climaxes around the Middle Triassic, Late Jurassic and Late Cretaceous (Berberian and Berberian, 1981). The distribution of Mesozoic plutonic bodies in Iran is mostly restricted to regions close to the eventual active plate margins marked by ophiolitic-melange belts. They appear to have been generated extensively along and above the early Mesozoic subduction zone of the Sanandaj-Sirjan zone.

Arc magmatism provides useful insights into mantle or crust melting processes in subduction zones (e.g., Pearce *et al.*, 1990; Davidson, 1996; Macdonald *et al.*, 2000), and in the case of Zagros, it should also help to solve some first-order geodynamic problems, such as: (1) The shift of ~300 km of subduction-related magmatism from the Mesozoic SSMA to the Tertiary UDMA. Does this result from a change in subduction processes (e.g., a change in slab dip; Berberian and Berberian, 1981) or from the existence of two distinct subduction zones? (2) The geochemical nature and significance of the recent, Upper Miocene to Plio-Quaternary

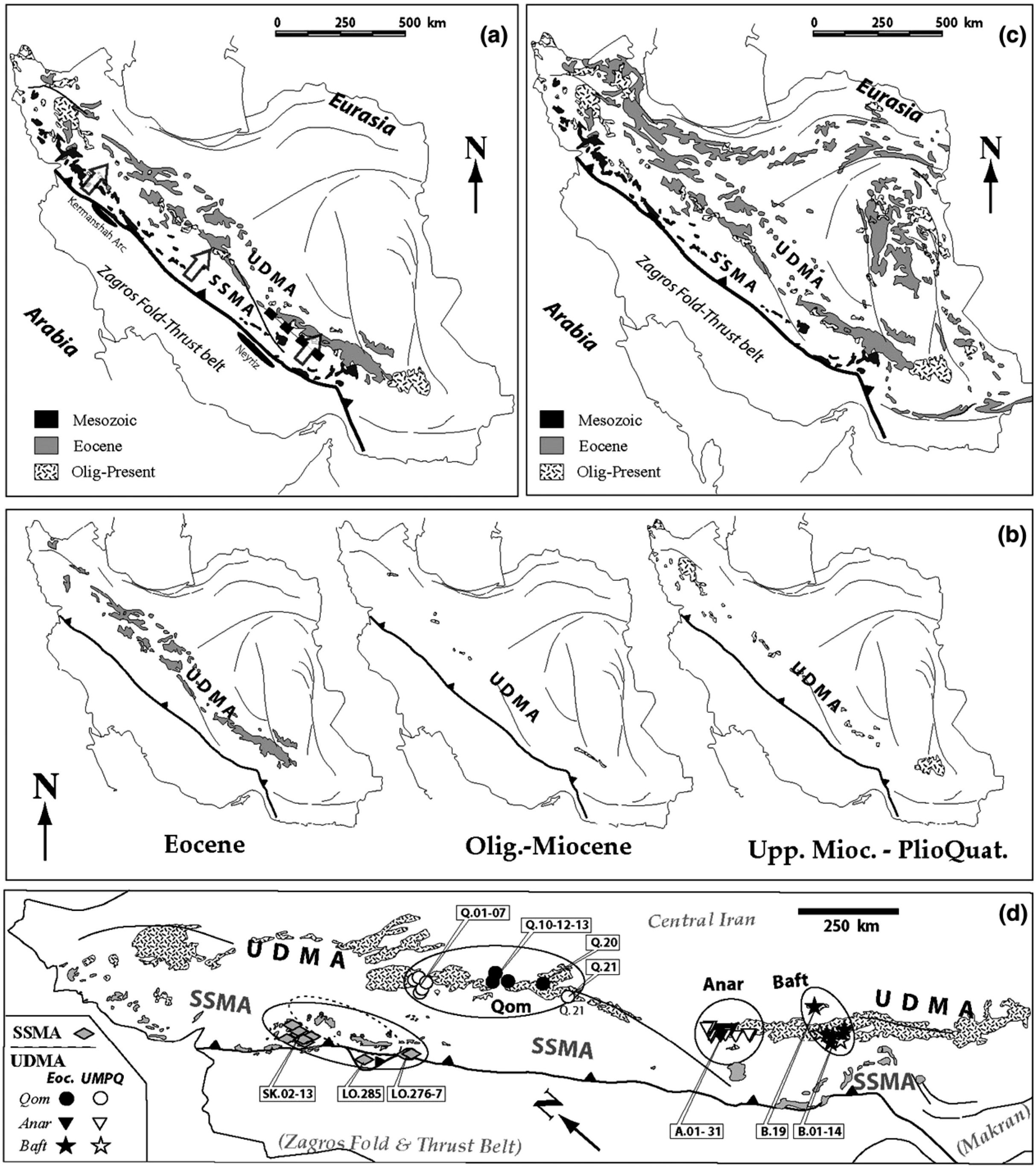

Figure 4. Maps showing the distribution of magmatic rocks in Iran (SSMA and UDMA: Sanandaj-Sirjan and Urumieh-Dokhtar magmatic arcs, respectively) (Omrani *et al*., 2008).

These maps were redrawn from the geological 1/2,500,000 scale map of Iran after careful checks on more detailed available geological maps (scale 1/250,000; Geological Survey of Iran). (a) Volcanic rocks in the SSMA and the UDMA. Volcanic and plutonic rocks of the SSMA are of Mesozoic age, whereas UDMA volcanic rocks start from the Eocene onwards. This magmatic shift in time and space is marked with arrows. (b) Distribution of the UDMA volcanic rocks through time, showing two prominent stages of magmatic activity during the Eocene and the Plio-Quaternary. (c) Distribution of Tertiary igneous rocks throughout Iran, showing that the Eocene magmatic activity is widespread and not restricted to the UDMA. Its origin remains largely unknown. (d) Sampling localities in both the SSMA and UDMA with three age groups: 1) SSMA volcanic rocks of Jurassic or Jurassic-Cretaceous age (grey symbols); 2) pre-collisional Eocene volcanics of the UDMA (black symbols); 3) Upper Miocene to Plio-Quaternary volcanic rocks of the UDMA post-dating the onset of collision (white symbols). Extensive sampling in the UDMA covers approximately half of the arc, from three main areas (from north to south: Qom, Anar and Baft regions). See Supplementary data for GPS locations.

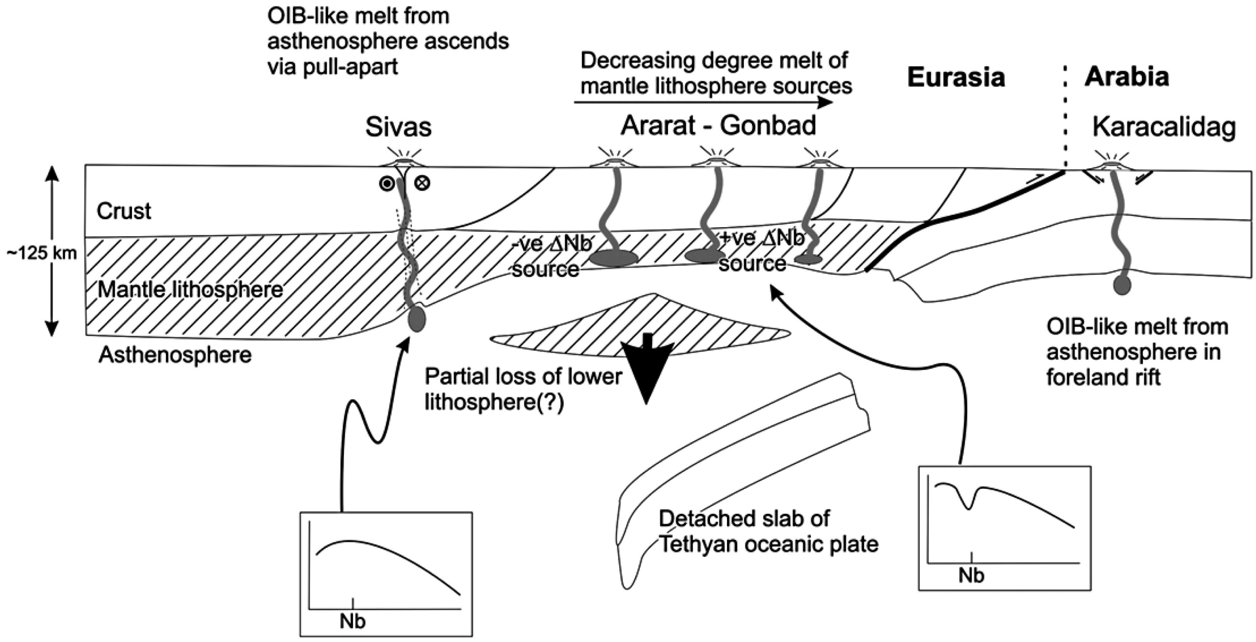

Figure 5. Schematic reconstruction for Quaternary volcanism across the Arabia-Eurasia collision zone and its foreland, in the region of NW Iran and eastern Turkey (Kheirkhah *et al.*, 2009).
Volcanic centre names are included to give examples for each setting of magmatism, and do not fall on a linear section line. Inset cartoons show spider diagrams of basalts derived from asthenosphere and mantle lithosphere sources.

magmatic activity postdating the onset of collision (c. 25 Ma; Agard *et al.*, 2005).

The Triassic plutonic rocks are well exposed in the southeastern part of the Sanandaj-Sirjan zone in the Sirjan and Esfandagheh area. The absence of these rocks in the central and northwestern sections of this zone is probably either due to their being covered by Jurassic and Cretaceous sedimentary rocks or because subduction of Neo-Tethys started from the southeast and propagated northward (Berberian and Berberian, 1981). Berberian and Berberian, 1981 suggested that the Triassic plutonic rocks might form as a result of steeply dipping Neo-Tethys oceanic slab (Mariana-type) underneath southeastern Central Iran.

V. Plutonic activity

Two magmatic belts dominated by calc-alkaline igneous rocks (Berberian and Berberian, 1981) run parallel to the Main Zagros Thrust on the Eurasian upper plate and cut across central Iran (Fig. 4a). The magmatic activity was restricted to the Sanandaj-Sirjan magmatic arc (SSMA) during the Mesozoic and to the Urumieh-Dokhtar magmatic arc during the Tertiary (UDMA; Fig. 4a).

Subduction inception dates back to the Late Triassic-Early Jurassic (Berberian and Berberian, 1981; Arvin *et al.*, 2007). The oldest magmatic rocks in the SSMA comprise the 199 ± 3 Ma Siah Kuh pluton (Arvin *et al.*, 2007) and several other plutons of Triassic age (Berberian and Berberian, 1981; Eshraghi and Jafarian, 1996; Sahandi, 2006). No age constraints younger than 65 Ma were found in the SSMA (Braud and Bellon, 1974; Valizadeh and Cantagrel, 1975; Sheikholeslami *et al.*, 2003; Ahmadi Khalaji *et al.*, 2007).

To the northeast of the SSMA, the parallel Urumieh-Dokhtar magmatic arc (Stöcklin, 1968; Alavi, 1994) forms an elongate volcanoplutonic belt running from eastern Turkey to southeast Iran and has been interpreted as subduction-related (Takin, 1972; Berberian and Berberian, 1981; Berberian *et al.*, 1982). The finding of rare, spatially restricted alkaline or shoshonitic volcanic rocks in this zone, however, led to alternative and contradictory interpretations (Amidi *et al.*, 1984; Hassanzadeh, 1993; Aftabi and Atapour, 2000).

VI. Young volcanic activity

Quaternary volcanic activity, generated by a complex combination of geodynamic and petrogenetic processes associated with the evolution of the Alpine-Himalayan collision belt, has occurred in a broad area running from west-to-east though Turkey, Iran and into Pakistan (Fig. 5). This volcanic activity has produced both andesitic stratovolcanoes, such as Ararat in Turkey (Kheirkhah *et al.*, 2009; Pearce *et* *al*., 1990) and Damavand in Iran (Davidson *et al*., 2004; Liotard *et al*., 2008), as well as fields of basaltic cones and plateau lavas.

In eastern Iran, the area of Quaternary magmatic activity extends over a south-to-north distance of 900 km, from the Makran arc in the south (Fig. 1; Farhoudi and Karig, 1977) to north of the northern margin of the Lut microcontinental block (Saadat, 2010; Saadat *et al*., 2010). The Makran volcanic arc, which consists of the Bazman (Salkhi, 1997) and Taftan (Biabangard and Moradian, 2008) stratovolcanoes in southeastern Iran, and the Koh-e-Sultan volcano in southwestern Pakistan (Nicholson *et al*., 2010), is produced by plate convergence involving the subduction of Oman Sea oceanic lithosphere beneath the Eurasian continent (Farhoudi and Karig, 1977). This relatively short volcanic arc segment is one of the simpler of the many different magmatic active sections of the Alpine-Himalayan collision belt, but only very limited geochemical information is available for these volcanoes. Bazman volcano, in addition to having erupted intermediate and silicic magmas, is surrounded by an extensive field of small mafic monogenetic Quaternary cones and associated lava flows. This paper presents petrochemical data for and discusses

1. Mesozoic SSMA and Eocene UDMA

SSMA Jurassic volcanics comprise andesites and basaltic andesites, together with some felsic tuffs and pyroclastics and so vary considerably in composition and texture (Table 1). UDMA volcanic rocks range from basalt to dacite and minor rhyolite. The Eocene samples show the widest range in composition (Table 2) and comprise andesite and intermediate tuff/pyroclastics, with minor basalts and dacites and rare rhyolites.

2. Upper Miocene to Plio-Quaternary (UMPQ) UDMA

Upper Miocene to Plio-Quaternary volcanic rocks postdating collision are less variable in composition. Andesites are abundant in the Qomand Baft regions, whereas in the central UDMA, near Anar, more differentiated rocks are found (trachyte, dacite, and rhyolite).

The petrography in intermediate and evolved rocks is dominated by plagioclase, amphibole and Fe-Ti oxides. Subcalcic augite is rare in these volcanic rocks, and is mostly found in phonolites and basaltic andesites. Biotite only occurs sporadically. Minor oxides (<5%), mainly titanomagnetite and very rarely hemoilmenite, are present in all samples. K-feldspar can be abundant in dacite, trachyte and rhyolite (e.g., A.05-06-07-08, Q.01-02).

3. UMPQ volcanics from Anar

All samples are slightly porphyritic with pheno- to mesocrysts of plagioclase, amphibole, biotite and rare pyroxene (Omrani *et al*., 2008). They also commonly contain titanomagnetite and apatite. Their composition varies from andesite to dacite. Plagioclase is the most abundant phenocryst in most samples and generally exhibits normal zoning patterns, but oscillatory zoning is also found occasionally (A.06). The oscillatory zoning might reflect some complex processes at the crystal-liquid interface during super cooling conditions at lower temperatures (L' Heureux and Fowler. 1996). The wide range in anorthite (An) content of normally zoned plagioclases (An55 to An30 from core to rim) is classically interpreted as disequilibrium under fast cooling in a magma undergoing decreasing water pressure (e.g., Gill, 1981, p. 169). The unusually low An content of most of the samples with respect to average calc-alkaline magmas could indicate a lower liquidus temperature under relatively low water pressures (Sisson and Grove, 1993; Scaillet and Evans, 1999).

Amphiboles are calcic to sodic-calcic in composition and mainly lie in the field of pargasite to edenite (Leake *et al*., 1997). Amphiboles from A.05d and A.06 show no clear chemical zoning. Pressure estimates based on Al-in-hornblende barometers (Hammarstrom and Zen, 1986; Johnson and Rutherford, 1989; Schmidt, 1992), suggest that these amphiboles formed at c. 5 and 2-3 kbar, respectively, thus excluding a mantle origin.

4. UMPQ volcanic rocks from Qom and Baft

These rocks mainly consist of basalts and basaltic andesites (B.01). The An content of plagioclase is relatively high in the pyroxene-rich basaltic andesites (e.g., An97 to 67; sample Q.21). In sample B.01 there is an obvious core-to-rim zonation, from high temperature pargasite to lower temperature edenite, respectively, with an evolution along both Si-Al and Fe-Mg solid solutions (Table 2). Pressure estimates suggest that this zoning took place between 8 and 5 kbar. One sample from the UDMA comprises orthopyroxene and clinopyroxene (Q.21) of enstatite and diopside compositions, respectively.

5. Makran volcanic arc

The two large dormant Neogene/Quaternary Bazman and Taftan stratovolcanoes form the western part of the Makran volcanic arc along the southern part of the Lut block and Sistan suture zone, southeastern Iran (Fig. 1). K-Ar ages for basalts from Bazman indicate that these rocks were erupted at

Table 1. Major and trace element data for 62 samples (Omrani *et al*., 2008).

	SSMA volcanics											Eocene volcanics (UDMA)																
												Qom				Anar					Baft							
	LO276	LO277	LO285	SK02	SK03	SK04	SK05	SK06	SK07	SK10	SK13	Q.10	Q.12	Q.13	Q.20	A.16	A.17	A.18	A.19	A.23	B.04	B.05	B.06	B.09	B.10	B.11	B.12	B.19
	*									*																		
SiO_2	62.54	58.71	47.35	75.71	78.28	79.06	68.37	50.74	48.53	61.38	71.53	48.58	69.73	73.70	58.84	61.26	54.03	53.50	53.97	55.77	54.28	50.89	53.96	54.36	52.37	51.46	68.76	61.25
TiO_2	0.67	0.61	1.08	0.18	0.29	0.18	0.52	2.96	1.20	0.46	0.39	1.43	0.50	0.19	0.66	0.52	0.73	0.70	0.69	0.96	0.81	0.76	1.59	0.88	0.68	0.85	0.22	1.19
Al_2O_3	16.55	17.67	15.20	12.26	4.86	12.26	15.43	14.30	16.86	14.78	14.24	17.42	13.85	12.54	14.93	16.28	18.99	18.99	18.78	18.30	19.06	19.50	13.85	19.13	19.03	19.00	14.45	16.61
Fe_2O_3	2.06	1.76	2.48	0.49	0.52	0.22	1.39	1.5	2.39	1.7	0.7	2.94	1.31	0.54	1.95	1.3	1.6	1.73	1.43	2.02	2.38	2.52	3.96	2.28	2.3	2.61	0.74	1.47
FeO	4.32	3.69	5.21	1.02	1.08	0.46	2.92	3.15	5.02	3.56	1.48	6.17	2.75	1.13	4.1	2.72	3.36	3.62	3.00	4.25	5.00	5.28	8.3	4.78	4.83	5.48	1.58	3.09
MnO	0.06	0.05	0.13	0.003	0.16	0.004	0.08	0.23	0.17	0.10	0.03	0.13	0.03	0.04	0.23	0.05	0.15	0.12	0.09	0.12	0.13	0.26	0.22	0.12	0.16	0.18	0.09	0.07
MgO	2.70	3.31	1.78	0.01	0.60	0.34	0.96	1.80	4.23	2.28	0.23	3.79	0.59	0.30	4.59	2.25	2.34	1.58	1.25	1.81	2.40	2.34	3.75	2.23	4.13	4.00	0.68	2.04
CaO	3.19	2.59	10.18	0.07	6.12	0.11	0.51	9.16	7.62	1.00	0.14	10.19	3.58	1.29	2.91	5.92	4.12	3.98	3.71	7.26	7.13	8.11	7.51	8.86	8.02	7.58	3.49	3.30
Na_2O	1.30	5.86	4.81	0.54	0.78	0.58	5.26	6.39	3.56	3.75	0.39	3.39	2.37	1.72	4.24	3.56	5.26	5.91	5.40	4.31	3.62	3.71	3.03	3.82	2.42	3.47	1.87	3.30
K_2O	2.18	1.61	1.31	9.24	1.09	4.40	2.23	0.32	0.93	1.52	8.89	1.55	3.53	5.78	2.89	3.71	4.81	4.23	5.67	0.77	0.95	0.96	0.91	0.18	1.42	0.12	2.38	3.39
P_2O_5	0.14	0.25	0.25	0.05	0.05	0.04	0.18	1.10	0.34	0.12	0.07	0.67	0.10	0.04	0.12	0.20	0.37	0.49	0.39	0.28	0.12	0.19	0.32	0.20	0.14	0.19	0.07	0.23
LOI	4.02	2.63	8.87	0.44	5.68	1.92	1.84	6.92	7.16	7.71	1.55	2.04	0.41	1.95	4.09	0.67	2.75	3.61	4.13	3.01	3.18	3.43	1.35	2.38	2.90	3.95	4.82	3.32
Total	99.73	98.75	98.65	100.01	99.53	99.59	99.69	98.57	98.00	98.36	99.64	98.31	98.75	99.21	99.55	98.44	98.50	98.45	98.46	98.85	99.06	97.96	98.76	99.22	98.40	98.89	99.13	99.26
Sr	339	572	294	10	44	12	65	188	242	191	49	636	176	54	125	465	611	645	895	367	432	504	273	408	400	429	124	248
Ba	346	174	112	407	208	404	225	98	187	68	880	545	657	643	532	666	979	1189	1116	335	231	417	111	145	248	194	1006	317
Y	24	18	28	16	14	15	53	65	26	18	44	30	43	18	21	17	23	23	23	30	21	21	43	28	18	25	16	29
Zr	137	113	136	125	101	124	465	298	144	82	402	126	256	120	168	163	194	161	194	195	77	58	126	128	82	90	131	221
Co	14	11	19	0	6	0	8	8	31	12	1	23	3	1	16	15	12	11	9	16	18	14	25	15	19	21	3	13
V	129	116	168	10	34	11	48	181	185	120	19	305	31	7	150	131	110	98	79	130	193	143	414	206	185	211	25	110
Ni	30	19	24	8	20	7	16	22	70	21	8	36	2	0	13	57	6	3	4	7	3	3	9	14	17	12	5	15
Cr	35	13	77	13	36	4	22	7	140	40	6	114	0	0	42	180	10	3	5	13	1	1	2	14	12	11	3	49
Zn	91	54	55	57	40	30	75	88	72	80	74	113	24	13	144	183	61	69	59	50	93	83	126	77	161	105	135	105
Cu	11	21	7	6	30	8	4	7	29	51	6	30	4	2	2	27	77	61	72	31	182	127	19	870	51	14	18	27
Sc	16	13	24	3	5	3	9	23	24	18	7	27	13	2	23	15	8	7	6	17	27	22	43	22	20	23	4	18
Rb	43.62	21.38	31.40	121.49	32.72	109.37	81.90	7.69	28.69	34.83	218.84	28.68	91.81	155.95	94.26	165.62	99.30	114.77	206.97	10.52	19.04	7.99	13.84	2.63	33.01	1.21	49.42	104.58
Nb	7.38	4.43	5.77	8.01	4.98	9.81	19.83	30.98	11.09	2.80	23.47	27.84	12.58	15.84	6.72	4.74	11.45	11.08	12.10	5.44	2.66	1.51	2.57	2.93	3.01	1.83	3.00	6.65
Mo	1.12	1.16	1.09	–	–	–	–	–	–	–	–	1.74	0.76	1.05	0.63	2.77	3.15	2.68	2.59	1.44	–	–	–	–	–	–	–	–
Sn	1.48	0.97	1.40	0.05	0.44	1.18	5.91	2.42	1.21	0.09	3.21	1.03	2.34	1.35	0.78	1.24	2.36	2.07	2.45	1.54	0.07	–	0.28	1.91	–	–	–	2.76
Sb	0.23	0.12	0.14	1.09	0.62	0.75	1.25	1.75	0.61	0.42	0.85	0.13	1.24	2.12	2.04	0.74	0.43	0.30	0.46	0.15	0.23	–	–	0.36	1.13	0.22	0.85	0.17
Cs	3.40	1.41	1.89	1.06	1.68	6.29	5.63	0.11	4.24	0.86	1.75	0.09	2.57	4.23	2.08	6.70	18.02	11.52	39.74	0.33	0.97	1.70	0.13	0.31	1.54	0.19	4.56	4.76
La	19.48	16.47	11.2	18.4	10.66	22.14	37.84	35.98	16.02	7.65	24.09	29.89	23.42	36.46	16.32	24.64	355.51	32.32	32.81	13.18	5.96	7.57	8.69	7.74	10.32	5.73	13.32	18.94
Ce	39.01	32.94	24.45	28.43	22.77	35.56	78.20	74.23	33.01	15.63	45.73	56.44	49.23	59.23	32.62	41.47	63.74	60.76	61.83	62.60	13.34	16.23	22.01	18.08	20.44	13.44	24.26	41.69
Pr	4.95	4.28	3.32	2.99	2.59	3.53	9.15	9.96	4.21	1.95	5.25	6.79	6.09	5.86	3.87	4.87	7.66	7.22	7.47	4.60	1.86	2.23	3.39	2.57	2.49	1.95	2.70	5.03
Nd	19.88	17.81	14.76	9.83	10.22	11.39	35.02	44.37	17.87	7.88	19.33	27.60	25.42	19.67	15.35	18.92	29.24	27.72	27.72	21.04	8.83	10.27	16.52	11.65	10.04	9.15	9.51	19.98
Sm	4.48	3.80	3.88	1.68	2.10	2.10	7.74	10.69	4.28	1.77	4.36	6.02	6.01	3.32	3.41	3.98	5.64	5.31	5.67	5.31	2.45	2.75	4.88	3.08	2.32	2.61	1.79	4.29
Eu	1.24	1.22	1.18	0.22	0.43	0.30	1.44	2.65	1.37	0.46	1.00	1.90	1.24	0.52	1.05	1.14	1.41	1.42	1.42	1.50	0.88	1.03	1.46	1.01	0.78	0.91	0.49	1.00
Gd	4.06	3.25	4.01	1.36	1.83	1.75	7.37	11.53	4.28	1.78	4.59	5.54	6.02	2.79	3.12	3.40	4.77	4.69	4.70	5.44	2.65	2.76	5.47	3.24	2.19	2.60	1.59	3.83
Tb	0.62	0.49	0.68	0.22	0.28	0.28	1.25	1.86	0.69	0.28	0.77	0.80	1.00	0.43	0.51	0.57	0.78	0.75	0.75	0.90	0.45	0.43	0.90	0.55	0.32	0.44	0.25	0.61
Dy	3.96	3.05	4.38	1.47	1.78	1.68	8.48	12.18	4.37	2.10	5.31	5.02	6.86	2.73	3.27	3.34	4.56	4.21	4.46	6.05	3.09	2.88	6.09	3.70	2.17	3.12	1.64	3.86
Ho	0.87	0.63	1.01	0.34	0.37	0.37	1.91	2.66	0.94	0.50	1.23	1.12	1.57	0.67	0.72	0.71	0.96	0.85	0.91	1.29	0.71	0.67	1.32	0.83	0.48	0.69	0.39	0.82
Er	2.21	1.60	2.63	0.97	1.00	0.99	5.40	6.60	2.44	1.33	3.27	2.71	4.06	1.87	2.01	1.86	2.57	2.25	2.47	3.36	1.82	1.73	3.58	2.32	1.26	1.81	1.11	2.02
Tm	0.34	0.25	0.40	0.18	0.16	0.17	0.90	0.98	0.36	0.21	0.57	0.41	0.63	0.32	0.31	0.32	0.45	0.37	0.42	0.57	0.28	0.25	0.52	0.37	0.20	0.29	0.18	0.32
Yb	2.14	1.54	2.48	1.2	0.97	1.24	6.06	5.85	2.37	1.44	3.74	2.67	4.21	2.46	2.06	2.11	2.97	2.49	2.76	3.41	1.77	1.76	3.39	2.34	1.14	1.81	1.28	1.93
Lu	0.36	0.26	0.40	0.21	0.15	0.20	0.96	0.90	0.34	0.23	0.59	0.42	0.67	0.39	0.35	0.31	0.41	0.35	0.41	0.50	0.29	0.30	0.59	0.38	0.19	0.32	0.22	0.30
Hf	3.96	3.08	3.64	2.50	2.36	3.03	10.70	7.12	3.29	1.85	8.12	3.23	7.93	4.11	4.13	3.96	4.94	3.59	4.41	4.94	2.07	1.42	2.97	2.87	1.81	1.92	3.04	4.02
Ta	0.57	0.31	0.42	1.11	0.40	1.21	1.53	2.25	0.81	0.20	1.97	1.70	1.09	1.70	0.54	0.39	0.64	0.61	0.63	0.43	0.18	0.09	0.19	0.20	0.20	0.14	0.33	0.65
W	0.68	0.40	0.80	2.06	–	–	–	–	1.40	–	0.82	4.01	2.28	2.42	2.17	1.58	1.89	1.69	2.48	0.78	1.09	0.35	0.45	1.22	1.14	0.79	1.47	1.73
Pb	9.87	6.38	3.16	5.64	11.09	71.13	10.08	7.29	22.28	7.09	8.02	15.98	8.26	5.96	14.28	19.30	32.69	32.09	33.37	7.45	5.21	7.54	2.96	8.36	8.29	6.54	17.04	12.47
Th	5.73	4.08	1.75	14.03	3.22	14.39	11.47	4.83	2.89	2.37	15.32	3.94	12.98	18.26	6.12	9.65	16.89	13.79	16.77	2.74	1.65	1.42	1.59	0.85	2.87	0.75	8.02	8.36
U	1.50	0.73	0.51	3.01	0.78	3.73	3.14	1.87	0.85	0.62	3.12	2.04	3.53	3.46	1.61	2.67	5.45	3.63	6.25	1.02	0.55	0.32	0.48	0.24	0.63	0.24	1.95	2.39
La/Yb	9	11	5	15	11	18	6	6	7	5	6	11	6	15	8	12	11	13	12	4	3	4	3	3	9	3	10	10
Sr/Y	14	32	11	1	3	1	1	3	9	11	1	21	4	3	6	27	26	28	39	12	20	24	6	15	23	17	8	8

* stands for recalculated value. Five samples of SSMA volcanic rocks showing a moderate alternation and a high loss on ignition (LOI>5 wt.%) were removed from major element data. All samples were included in the trace element data, however, because HREE elements are known to be relatively insensitive to alteration.

Table 1. continued

	Miocene to Plio-Quaternary volcanics (UDMA)																
	Qom									Anar							
	Q01a	Q01c	Q02a	Q02b	Q04	Q05	Q06a	Q07	Q21	A01	A03	A05a	A05c	A05d	A05e	A06	A07
SiO_2	52.47	61.86	51.50	50.50	62.07	54.21	62.68	55.87	56.97	63.62	63.80	74.15	73.90	73.57	74.07	65.54	68.12
TiO_2	0.89	0.46	0.89	1.26	0.58	0.95	0.42	0.60	0.54	0.46	0.44	0.19	0.18	0.18	0.18	0.50	0.44
Al_2O_3	20.07	16.52	17.06	17.25	15.80	17.38	16.99	16.79	19.01	16.19	15.38	13.96	13.43	13.77	13.81	16.59	1576
Fe_2O_3	2.29	1.70	2.80	3.20	1.6	2.63	1.38	1.91	1.77	1.27	1.04	0.46	0.45	0.44	0.46	1.18	1.07
FeO	4.82	3.56	5.88	6.72	3.36	5.53	2.9	4.00	3.72	2.67	2.18	0.96	0.95	0.92	0.96	2.48	2.26
MnO	0.13	0.11	0.14	0.12	0.15	0.12	0.02	0.07	0.09	0.09	0.06	0.03	0.03	0.03	0.02	0.07	0.02
MgO	2.56	1.75	5.22	4.74	2.69	3.85	2.47	3.29	3.39	0.78	1.60	0.27	0.30	0.31	0.22	1.49	0.39
CaO	7.92	5.24	8.24	9.41	4.79	8.47	5.44	7.32	7.70	5.79	4.38	2.28	1.79	1.93	1.93	4.69	3.53
Na_2O	3.90	3.56	2.74	2.87	3.94	3.06	4.19	2.93	3.26	4.14	4.29	4.12	4.05	3.99	4.24	5.12	4.81
K_2O	0.63	1.28	0.61	0.20	2.47	1.06	0.78	1.33	1.56	1.90	2.16	2.95	2.89	3.26	2.99	1.98	2.10
P_2O_5	0.22	0.28	0.17	0.22	0.18	0.17	0.16	0.14	0.20	0.31	0.20	0.07	0.07	0.07	0.09	0.22	0.24
LOI	2.35	2.07	3.55	1.44	0.88	1.17	2.46	4.60	0.41	2.17	3.73	0.71	1.81	1.81	0.49	0.22	0.94
Total	98.26	98.38	98.81	97.93	98.52	98.60	99.88	98.87	98.62	99.38	99.26	100.14	99.86	100.29	99.47	100.08	99.68
Sr	447	389	497	330	417	353	536	471	965	898	739	358	343	372	354	875	960
Ba	380	376	200	199	927	313	205	182	444	775	630	658	648	657	638	584	676
Y	26	22	19	27	19	23	14	19	12	12	8	4	4	4	5	9	7
Zr	93	107	56	86	138	109	90	87	93	155	116	122	120	123	131	113	128
Co	17	6	27	28	12	24	8	14	17	11	9	2	2	2	2	10	8
V	162	30	246	267	113	252	66	120	130	89	71	16	16	17	17	82	66
Ni	10	3	30	26	9	29	3	7	20	16	20	0	0	0	4	15	16
Cr	2	0	44	37	19	15	0	12	21	26	19	0	0	0	9	16	20
Zn	71	84	62	58	216	81	34	17	59	67	49	26	28	30	53	55	87
Cu	15	6	13	100	23	35	7	13	37	48	36	9	10	17	11	35	37
Sc	18	7	28	31	12	27	8	15	13	8	5	-	-	-	-	6	5
Rb	6.60	19.25	12.50	1.50	88.35	26.75	24.41	30.42	25.71	50.45	41.51	87.56	82.60	84.23	76.91	41.10	45.91
Nb	4.23	4.49	2.07	3.08	7.61	4.10	3.69	4.00	3.01	5.97	5.83	3.60	3.48	3.67	3.43	4.64	6.35
Mo	1.31	1.55	1.31	1.44	1.76	1.65	1.14	1.05	0.05	2.55	1.15	2.11	3.30	2.76	1.92	1.50	1.74
Sn	1.14	1.23	0.85	1.34	1.41	1.28	0.51	0.85	0.83	1.28	0.95	0.68	0.97	0.84	0.88	1.05	1.01
Sb	0.13	0.17	0.65	0.23	0.47	0.67	0.07	0.07	0.09	0.19	0.32	0.47	0.33	0.37	0.31	0.38	0.50
Cs	0.13	0.10	1.31	0.08	2.45	0.38	0.42	2.39	0.38	1.45	2.86	3.14	3.74	3.71	2.31	1.66	11.32
La	15.72	18.92	10.78	13.25	32.31	16.32	13.19	10.86	11.81	32.06	27.61	23.02	23.39	22.89	21.97	19.09	32.99
Ce	31.07	37.82	21.56	27.24	56.45	33.18	26.88	23.88	24.30	59.16	50.61	40.38	41.30	40.37	38.75	38.15	58.39
Pr	3.90	4.56	2.80	3.52	5.99	4.13	3.27	3.08	3.16	6.83	5.62	4.37	4.51	4.49	4.18	4.74	6.70
Nd	16.54	18.34	12.15	15.48	21.22	17.05	13.08	12.88	12.76	25.15	19.78	15.02	15.38	15.13	14.56	18.73	23.87
Sm	4.25	4.13	3.08	4.17	3.91	3.86	2.65	3.27	2.76	4.40	3.27	2.33	2.36	2.36	2.29	3.50	3.80
Eu	1.30	1.24	1.03	1.21	1.09	1.07	0.90	0.75	0.90	1.35	0.91	0.62	0.65	0.65	0.60	1.01	1.15
Gd	3.96	3.69	3.11	4.13	3.40	3.76	2.37	3.17	2.42	3.57	2.39	1.49	1.69	1.67	1.38	2.59	2.75
Tb	0.62	0.56	0.51	0.69	0.51	0.60	0.37	0.51	0.34	0.46	0.32	0.19	0.19	0.19	0.17	0.35	0.34
Dy	4.07	3.52	3.20	4.55	3.09	3.79	2.16	3.27	2.14	2.45	1.54	0.85	0.92	0.88	0.81	1.83	1.54
Ho	0.91	0.77	0.72	0.99	0.66	0.82	0.49	0.70	0.44	0.46	0.30	0.16	0.16	0.15	0.13	0.35	0.28
Er	2.36	2.11	1.90	2.59	1.78	2.16	1.32	1.82	1.18	1.18	0.74	0.37	0.40	0.36	0.37	0.82	0.67
Tm	0.36	0.33	0.28	0.37	0.27	0.29	0.21	0.26	0.17	0.19	0.12	0.06	0.06	0.06	0.05	0.13	0.11
Yb	2.23	2.06	1.70	2.37	1.73	2.07	1.40	1.76	1.07	1.11	0.70	0.34	0.36	0.35	0.32	0.82	0.64
Lu	0.35	0.35	0.29	0.38	0.30	0.34	0.24	0.28	0.18	0.15	0.10	0.05	0.06	0.05	0.05	0.12	0.09
Hf	2.84	3.41	1.80	2.72	4.20	3.31	2.70	2.68	2.51	3.74	3.15	3.62	3.57	3.63	3.39	3.10	3.51
Ta	0.29	0.34	0.15	0.23	0.69	0.31	0.26	0.27	0.20	0.42	0.35	0.35	0.34	0.33	0.33	0.31	0.39
W	0.85	3.41	1.69	0.99	3.47	1.67	0.86	0.57	0.94	1.15	0.71	1.27	1.10	1.02	0.58	0.73	3.57
Ph	6.63	4.34	6.99	6.92	91.07	8.50	5.30	5.30	6.51	23.07	12.71	19.66	19.98	20.06	18.53	13.96	15.68
Th	4.03	5.01	2.73	3.80	19.82	6.27	2.73	2.84	1.97	11.09	6.99	6.67	7.50	7.64	7.31	3.82	8.98
U	1.13	1.40	0.81	0.99	1.69	1.57	0.76	0.81	2.09	3.18	1.85	2.53	2.61	1.90	1.34	2.47	2.30
La/Yb	7	9	6	6	19	8	9	6	11	29	39	67	65	66	69	23	52
Sr/Y	18	18	26	12	22	15	38	25	79	75	92	83	77	85	75	93	140

Table 1. continued

	Miocene to Plio-Quaternary volcanics (UDMA)																
	Anar														Baft		
	A08	A09	A13	A14	A20a	A20b	A21	A22	A26	A27	A28	A29	A30	A31	B01	B03	B14
SiO_2	68.51	65.02	67.13	66.91	71.29	70.25	71.39	70.48	66.30	65.06	60.30	62.31	66.76	59.90	58.69	57.90	56.40
TiO_2	0.43	0.42	0.42	0.40	0.29	0.31	0.28	0.31	0.50	0.40	0.49	0.45	0.42	0.61	0.48	0.63	0.79
Al_2O_3	15.73	15.36	16.42	15.24	15.13	15.23	14.56	15.01	16.71	16.20	17.15	17.70	16.55	16.69	18.29	17.87	17.05
Fe_2O_3	0.97	1.01	1.05	0.86	0.57	0.58	0.54	0.58	0.78	1.01	1.61	1.15	0.85	1.55	1.63	2.07	1.83
FeO	2.03	2.12	2.2	1.81	1.19	1.22	1.13	1.22	1.63	2.11	3.37	2.42	1.79	3.25	3.42	4.35	3.83
MnO	0.03	0.05	0.04	0.05	0.03	0.03	0.03	0.01	0.01	0.05	0.11	0.07	0.04	0.09	0.11	0.09	0.11
MgO	0.65	1.72	1.09	1.11	0.42	0.50	0.40	0.54	0.40	1.31	2.79	1.73	0.86	3.34	2.70	3.53	3.49
CaO	3.44	4.40	3.74	4.06	2.55	2.83	2.53	2.55	3.42	3.75	5.21	4.32	4.05	5.97	6.27	6.51	7.65
Na_2O	4.25	4.75	4.93	4.47	4.64	4.66	4.63	4.78	4.55	4.97	3.96	3.81	4.94	4.46	4.01	3.30	4.26
K_2O	2.56	2.16	2.18	2.40	2.73	2.70	2.70	2.64	2.68	2.31	1.98	2.43	2.53	2.34	1.33	2.03	2.16
P_2O_5	0.19	0.19	0.17	0.17	0.11	0.12	0.10	0.12	0.25	0.18	0.18	0.19	0.18	0.23	0.16	0.15	0.40
LOI	1.07	2.38	0.81	2.11	0.09	0.58	0.20	0.40	1.14	1.21	1.66	2.68	0.76	1.12	2.64	0.64	1.93
Total	99.85	99.59	100.17	99.60	99.05	99.00	98.48	98.63	98.36	98.54	98.81	99.27	99.74	99.55	99.74	99.07	99.89
Sr	540	765	831	623	504	505	501	492	834	746	628	867	812	921	598	374	922
Ba	571	758	643	562	584	552	555	522	586	670	521	803	596	784	237	284	576
Y	8	8	8	8	5	5	5	5	6	8	11	12	9	13	13	21	15
Zr	150	99	116	115	145	155	144	160	116	113	81	128	166	110	86	126	129
Co	6	8	8	8	4	3	3	3	4	8	15	10	6	17	14	17	16
V	60	70	64	55	31	27	31	30	68	59	103	69	53	113	115	160	141
Ni	13	20	6	7	0	0	0	0	5	3	15	11	4	46	16	12	58
Cr	17	21	8	16	2	8	3	2	14	5	17	52	10	103	14	16	134
Zn	43	37	46	118	26	43	41	41	17	28	55	176	47	45	78	54	100
Cu	39	68	49	29	25	26	39	25	7	17	31	42	36	32	28	23	53
Sc	4	5	5	3					2	5	10	7	4	11	11	18	13
Rb	63.11	41.55	59.46	63.53	69.86	61.70	60.77	59.09	54.95	56.32	55.73	51.47	49.66	47.65	40.60	68.84	41.53
Nb	5.50	5.92	5.26	5.60	2.68	2.65	2.46	2.84	5.93	4.05	2.73	5.81	5.31	6.64	2.28	3.73	10.68
Mo	0.83	1.43	1.94	1.55	1.55	0.72	0.46	0.94	1.27	0.44	0.48	0.80	2.13	0.46	–	–	
Sn	1.18	1.12	0.89	1.19	0.98	0.87	1.06	1.21	0.99	0.92	1.01	2.66	0.29	0.70	–	–	0.43
Sb	0.45	0.27	0.14	0.22	0.07	0.10	0.04	0.15	1.59	0.07	0.17	0.08	0.12	0.12	0.24	0.52	0.10
Cs	2.94	0.64	1.20	3.76	2.15	1.77	1.53	1.97	1.65	1.28	1.34	1.70	0.71	1.44	1.28	3.87	1.91
La	23.73	28.31	21.27	24.12	23.19	22.89	23.37	23.37	23.62	20.62	13.58	23.26	32.97	21.69	9.49	11.72	30.81
Ce	42.98	49.66	39.71	46.25	42.71	41.81	42.90	43.03	44.73	39.57	26.14	44.16	59.03	41.03	19.91	24.59	57.19
Pr	5.15	5.56	4.61	5.49	4.84	4.80	4.84	4.81	5.27	4.62	3.23	5.23	6.73	4.92	2.53	3.10	6.31
Nd	19.12	20.16	17.24	20.26	16.63	16.58	16.77	17.49	19.97	17.54	12.98	19.98	24.60	19.12	10.47	12.33	22.93
Sm	3.34	3.38	3.14	3.55	2.68	2.69	2.78	2.89	3.45	3.25	2.92	3.60	4.18	3.47	2.21	2.99	3.94
Eu	0.95	0.94	0.95	1.08	0.74	0.77	0.79	0.76	1.00	0.90	0.88	1.06	1.15	1.07	0.72	0.79	1.10
Gd	2.38	2.43	2.36	2.75	1.83	1.78	1.82	1.97	2.40	2.51	2.51	2.66	2.81	2.80	2.06	2.81	2.94
Tb	0.32	0.32	0.33	0.37	0.22	0.24	0.23	0.25	0.30	0.32	0.39	0.35	0.30	0.36	0.29	0.44	0.35
Dy	1.57	1.66	1.69	2.02	1.06	1.04	1.07	1.05	1.51	1.77	2.37	1.92	1.50	2.10	1.74	2.88	1.85
Ho	0.30	0.32	0.33	0.35	0.18	0.19	0.18	0.19	0.26	0.33	0.46	0.36	0.25	0.40	0.40	0.64	0.35
Er	0.73	0.77	0.81	0.86	0.46	0.45	0.43	0.45	0.66	0.89	1.27	0.93	0.60	1.02	0.98	1.68	0.90
Tm	0.12	0.11	0.12	0.14	0.06	0.07	0.08	0.08	0.11	0.13	0.21	0.14	0.08	0.16	0.15	0.25	0.13
Yb	0.71	0.74	0.77	0.83	0.43	0.43	0.44	0.49	0.72	0.86	1.34	0.92	0.51	0.98	0.99	1.68	0.79
Lu	0.10	0.10	0.12	0.11	0.06	0.07	0.07	0.07	0.10	0.11	0.20	0.15	0.08	0.16	0.16	0.27	0.13
Hf	3.66	2.84	3.40	3.58	3.68	3.66	3.62	4.05	3.20	2.91	2.41	3.37	4.37	2.89	2.20	2.99	2.48
Ta	0.41	0.39	0.37	0.45	0.25	0.26	0.23	0.25	0.43	0.33	0.22	0.46	0.35	0.49	0.19	0.28	0.75
W	1.93	1.29	0.86	1.22	3.15	1.34	0.91	0.83	3.54	2.20	1.17	2.40	1.20	1.10	2.72	1.55	3.42
Ph	17.54	12.40	15.09	16.16	15.83	16.58	14.69	15.51	25.71	10.25	32.48	16.51	14.02	12.93	8.84	9.24	12.15
Th	6.34	6.94	7.74	7.05	5.66	5.35	5.69	5.63	5.43	6.76	2.48	5.46	6.95	4.52	2.24	5.07	10.74
U	2.68	1.98	2.11	1.00	1.90	1.99	2.00	1.48	1.67	1.64	0.83	2.07	1.60	6.77	1.35	2.25	2.12
La/Yb	33	38	28	29	54	53	53	47	33	24	10	25	65	22	10	7	39
Sr/Y	65	94	104	77	112	103	110	103	135	90	58	72	94	68	47	18	64

Table 2. List of representative mineral analyses of amphibole (amph), pyroxene (px) and feldspar (fsp) in upper Miocene to Plio-Quaternary adakitic samples from the UDMA (Omrani *et al*., 2008).

Mineral	amph	amph	amph	amph	amph	amph	amph	amph	amph	px	px	px	fsp	fsp	fsp	fsp
											c		c	r	c	r
Sample	A.05d	A.06	A.06	A.06	A.06	B.01	B.01	B.01	B.01	Q.21	Q.21	Q.21	B.01	B.01	A.06	A.06
	f366	a2	a4	a48	a51	d223	d245	d247	d250	c130	c151	c158	d211	d219	a6	a7
SiO_2	43.00	47.56	46.63	48.27	48.74	41.78	42.35	43.46	43.24	52.60	51.04	48.65	54.02	55.85	59.32	60.90
TiO_2	0.79	0.68	0.90	0.65	0.56	0.97	0.86	0.65	0.60	0.07	0.21	0.39	0.01	0.02	0.01	0.01
Al_2O_3	10.55	6.48	7.41	8.16	5.51	14.46	12.58	11.46	11.13	2.53	2.64	4.55	28.82	26.93	25.115	23.96
FeO	15.79	12.46	12.49	10.26	11.87	12.01	13.67	14.09	15.39	15.98	8.26	8.94	0.18	0.15	0.22	0.26
MnO	0.17	0.31	0.45	0.33	0.41	0.22	0.23	0.33	0.65	0.41	0.28	0.17	0.00	0.04	0.01	0.03
MgO	12.37	15.83	15.12	14.13	15.98	13.23	12.50	12.83	12.23	26.63	15.78	14.40	0.01	0.00	0.01	0.02
CaO	10.81	10.93	10.80	11.64	11.14	11.59	11.00	11.04	10.52	1.40	20.27	20.85	10.80	8.67	6.63	5.39
Na_2O	1.97	1.49	1.89	2.16	1.37	1.96	1.82	1.65	1.60	0.02	0.27	0.36	5.38	6.21	7.17	7.85
K_2O	0.50	0.61	0.46	0.36	0.40	0.43	0.39	0.35	0.29	0.00	0.00	0.00	0.14	0.15	0.55	0.67
Sum	95.95	96.35	96.15	95.95	95.99	96.63	95.39	95.86	95.65	99.63	98.76	98.31	99.35	98.02	99.06	99.09
Structural formula																
Si	6.53	7.04	6.93	7.09	7.20	6.20	6.40	6.53	6.56	1.92	1.92	1.85	2.45	2.55	2.67	2.73
Ti	0.09	0.08	0.10	0.07	0.06	0.11	0.10	0.07	0.07	0.00	0.01	0.01	0.00	0.00	0.00	0.00
Al	1.89	1.13	1.30	1.41	0.96	2.53	2.24	2.03	1.99	0.11	0.12	0.20	1.54	1.45	1.33	1.27
FeO_{tot}	2.01	1.54	1.55	1.26	1.47	1.49	1.73	1.77	1.95	0.49	0.26	0.28	0.01	0.01	0.01	0.01
Mn	0.02	0.04	0.06	0.04	0.05	0.03	0.03	0.04	0.08	0.01	0.01	0.01	0.00	0.00	0.00	0.00
Mg	2.80	3.49	3.35	3.09	3.52	2.92	2.81	1.87	2.76	1.45	0.88	0.82	0.00	0.00	0.00	0.00
Ca	1.76	1.73	1.72	1.83	1.76	1.84	1.78	1.78	1.71	0.05	0.82	0.85	0.53	0.42	0.32	0.26
Na	0.58	0.43	0.55	0.62	0.39	0.56	0.53	0.48	0.47	0.00	0.02	0.03	0.47	0.55	0.63	0.68
K	0.10	0.11	0.09	0.07	0.08	0.08	0.07	0.07	0.06	0.00	0.00	0.00	0.01	0.01	0.03	0.04
XMg	0.58	0.69	0.68	0.70	0.70	0.66	0.62	0.61	0.58	0.74	0.77	0.74	0.14	0.01	0.06	0.10
NO*x*	23	23	23	46	46	46	46	46	46	6	6	6	8	8	8	8

Abbreviations: c- core, NOx- number of oxygens per formula unit, r- rim, Sample labels A, B, Q refer to Anar, Baft and Qom, respectively.

4.6 Ma and 0.6 Ma, respectively (Conrad *et al*., 1981). Taftan consists of pyroclastic, tuffs, ignimbrites and lava flows, including basalts, basaltic-andesites, andesites and dacites (Ghazban, 2004). Biabangard and Moradian (2008) determined, from K/Ar ages of selected andesitic and andesite-basalt samples that volcanic activity at Taftan began by at least 6.95 Ma and the youngest eruption probably occurred at b0.71 Ma. Also, 40Ar/39Ar ages of b0.8 and 2.6 Ma were obtained for two samples of andesitic lava on the northwestern flank of Taftan (Moinvazire, 1998). A lava flow was reported at Taftan in 1993, but may instead have actually been an observation of a molten sulfur flow (Siebert and Simkin, 2002). Koh-e-Sultan, located at the eastern end of the Makran volcanic arc in Pakistan, is less than 2.5 Ma in age (Siddiqui, 2004). It has a compositional range from basaltic andesites to dacites and a calc-alkaline fractionation trend (Biabangard and Moradian, 2008; Nicholson *et al*., 2010).

Ⅶ. Conclusions

The following conclusions can be drawn from the studies:

1. Subduction of the Tethyan oceanic lithosphere under the southwestern border of Central Iran, caused plutonic and volcanic activity between the Jurassic and Quaternary within and adjacent to the southern margin of Central Iran.
2. Two magmatic arcs of Mesozoic and Tertiary age, Sanandaj-Sirjan and Urumieh-Dokhtar magmatic arcs formed due to the convergence between Arabia and Eurasia along the strike of the Zagros Mountains. Magmatism was active during subduction and later resumed in the UDMA after the inception of collision, from the Late Miocene onwards.
3. The shift of the magmatic activity from the Mesozoic SSMA to the UDMA later in the Eocene is not well understood at present. Geochemical data however suggests that they both originated from typical, subduction-related mantle wedge sources.
4. After Late Miocene adakitic magma in some parts of the UDMA was formed. The presence and distribution of these mostly high-SiO_2 adakites imply that some subducted slab relicts melted at depth due to slab break-off.
5. Quaternary volcanic activity, generated by a complex combination of geodynamic and petrogenetic processes associated with the evolution of the Alpine-Himalayan collision belt. This volcanic activity has produced both andesitic stratovolcanoes and fields of basaltic cones and plateau lavas.
6. Upper Miocene to Pliocene-Quaternary volcanic activity is observable in Makran, UDMA, Qom-Baft, Anar and northern Lut.

Acknowledgments

Our special words of thanks go to the people whose guidance and assistance were indispensable in the successful completion of this study. The first author, Jamshid Ahmadian would like to express his deepest gratitude to Dr.Yuzo Tanaka, the President of Naruto University of Education, for awarding the research scholarship to him. He also thanks Dr. Ziari, the President of Payme Noor University, for his valuable support and contribution on this research. This work was supported by the foreign visiting researcher program 2012 of Naruto University of Education and the joint research project (O) of the joint graduate school(Ph.D. Program) in science of school education, Hyogo University of Teacher Education.

References

Aftabi, A., Atapour, T., 2000. Regional aspects of shoshonitic volcanism in Iran. Episodes 23, 119-125.

Agard, P., Omrani, J., Jolivet, L., and Mouthereau, F., 2005. Convergence history across Zagros (Iran): constraints from collisional and earlier deformation. International Journal of Earth Science, 94, 401-419.

Ahmad, T., and Posht Kuhi, M., 1993. Geochemisty and petrogenesis of Urumiah-Dokhtar volcanics around Nain and Rafsanjan areas: a preliminary study, Treatise on the Geology of Iran. Iranian Ministry of Mines and Metals, 90p.

Ahmadi Khalaji, A., Esmaeily, D., Valizadeh, M.V., Rahimpour-Bonab, H., 2007. Petrology and geochemistry of the granitoid complex of Boroujerd, Sanandaj-Sirjan Zone, Western Iran. Journal of Asian Earth Sciences 29, 859-877.

Alavi, M., 1980. Tectonostratigraphic evolution of the Zagrosides of Iran. Geology, 8, 144-149.

Alavi, M., 1994. Tectonics of the Zagros orogenic belt of Iran; new data and interpretations. Tectonophysics, 229, 211-238.

Allen, M., Jackson, J., and Walker, R., 2004. Late Cenozoic reorganization of the Arabia-Eurasia collision and the comparison of short-term and long-term deformation rates. Tectonics, 23, TC2008, 1-16.

Allen, M.B., Armstrong, H.A., 2008. Arabia-Eurasia collision and the forcing of mid Cenozoic global cooling.

Palaeogeography Palaeoclimatology Palaeoecology 265, 52-58.

Amidi, M., Emami, M.H., and Michel, R., 1984. Alkaline character of Eocene volcanism in the middle part of Iran and its geodynamic situation. Geologische Rundschau 73, 917-932.

Berberian, M., 1981. Active faulting and tectonics of Iran. In: H.K. Gupta and F.M. Delany (Ed.), Zagros-Hindu Kush-Himalaya Geodynamic evolution. American Geophys. Union, Geodyn. Ser., 3, 33-69.

Berberian, M., 1995. Master "blind" thrust faults hidden under the Zagros folds; active basement tectonics and surface morphotectonics. Tectonophysics, 241, 193-224.

Berberian, F., and Berberian, M., 1981. Tectono-Plutonic Episodes in Iran. Geological Survey of Iran, Rep. 52, 566-593.

Berberian, M., and King, G.C.P., 1981. Towards a paleogeography and tectonic evolution of Iran. Canadian Journal of Earth Sciences, 18, 210-265.

Berberian, M., Yeats, R., 1999. Patterns of historical earthquake rupture in the Iranian plateau. Bulletin of the Seismological Society of America 89, 120-139.

Berberian, F., Muir, I.D., Pankhurst, R.J., and Berberian, M., 1982. Late Cretaceous and early Miocene Andean-type plutonic activity in northern Makran and central Iran. Journal of the Geological Society of London, 139, 605-614.

Biabangard, H., Moradian, A., 2008. Geology and geochemical evaluation of Taftan Volcano, Sistan and Baluchestan Province, southeast of Iran. Chinese Journal of Geochemistry 27, 356-369.

Bina, M.M., Bucur, I., Prevot, M., Meyerfeld, Y., Daly, L., Cantagrel, J.M., and Mergoil, J., 1986. Palaeomagnetism petrology and geochronology of Tertiary magmatic and sedimentary units from Iran. Tectonophysics, 121, 303-329.

Blanc, E.J.P., Allen, M.B., Inger, S., and Hassani, H., 2003. Structural style in the Zagros Simple Folded Zone, Iran. Journal of the Geological Society, London, 160, 401-412.

Braud, J. and Bellon, H., 1974. Données nouvelles sur le demaine métamorphique du Zagros (zone de Sanandaj-Sirjan) au niveau de Kermanshah-Hamadan (Iran): nature âge et interprétation des séries métamorphiques et des intrusions; évolution structurale. Rapport Université Paris-Sud, 20 pp.

Conrad, G., Montignary, R., Thuizat, R., Westphal, M., 1981. Tertiary and Quaternary geodynamics of southern Lut (Iran) as deduced from palaeomagnetic, isotopic and structural data. Tectonophysics 75, 11-17.

Copley, A., Jackson, J., 2006. Active tectonics of the Turkish-Iranian Plateau. Tectonics 25.

Davidson, J.P., 1996. Deciphering mantle and crustal signature in subduction zone magmatism. In: Bebout, G.E., Scholl, D.W., Kirby, S.H., Platt, J.P. (Eds.), Subduction: Top to Bottom. American Geophysical Union, Washington DC, pp. 251-262.

Davidson, J., *et al*., 2004. The geology of Damavand volcano, Alborz Mountains, northern Iran. Geological Society of America Bulletin 116, 16-29.

Dewey, J.F., Pitman, W.C. III, Ryan, W.B.F., and Bonnin, J., 1973. Plate tectonics and the evolution of the Alpine System. Geological Society of America Bulletin, 84, 3137-3180.

Dewey, J.F., Hempton, M.R., Kidd, W.S.F., Saroglu, F., Şengör, A.M.C., 1986. Shortening of continental lithosphere: the neotectonics of Eastern Anatolia — a young collision zone. In: Coward, M., Ries, A. (Eds.), Collision Tectonics. Special Publication of the Geological Society, vol. 19, pp. 3-36. London.

Eshraghi, S.A., Jafarian, M.B., 1996. Geological Map of Songhor. Geological Survey of Iran.

Falcon, N.L., 1969. Problems of the relationship between surface structure and deep displacements illustrated by the Zagros range. In: Kent, P.E. (Ed.), Time and Place in Orogeny. Geological Society Special Publications, London, 3, 9-22.

Falcon, N., 1974. Zagros Mountains, Mesozoic-Cenozoic orogenic belts (edited by Spencer, A.), Special Publication of Geological Society, London, 4, 199-211.

Farhoudi, G., Karig, D.E., 1977. Makran of Iran and Pakistan as an active arc system. Geology 5, 664-668.

Forster, H., Fesefeldt, K., and Kursten, M., 1972. Magmatic and orogenic evolution of the central Iranian volcanic belt. 24th International Geology Congress, Section 2, 198-210.

Ghasemi, A., and Talbot, C.J., 2006. A new scenario for the Sanandaj- Sirjan zone (Iran). Journal of Asian Earth Sciences, 26, 683-693.

Ghazban, F., 2004. Alteration and geochemistry of Mount Taftan geothermal prospect southeastern Iran. Iranian International Journal of Science 5 (1), 43-62.

Gill, J., 1981. Orogenic Andesites and Plate Tectonics. Springer-Verlag, Berlin. 385pp.

Haghipour, A., and Aghanabati, A., 1985. Geologicla map of Iran, scale 1:2,500,000. Geological Survey of Iran.

Hammarstrom, J.M., Zen, E., 1986. Aluminium in hornblende: an empirical igneous barometer. American Mineralogist 71, 1297-1313.

Hassanzadeh, J., 1993. Metallogenic and tectonomagmatic events in the SE sector of the Cenozoic active continental margin of Iran (Shahre Babak area, Kerman Province). Unpublished PhD thesis, University of California, Los Angeles, 204p.

Haynes, S.J. and McQuillan, H., 1974. Evolution of the Zagros suture zone, southern Iran, Bulletin Geological Society of America, 85, 739-744.

Hessami, K., Koyi, H.A., Talbot, C.J., Tabasi, H., and Shabanian, E., 2001. Progressive unconformities within an evolving foreland fold-thrust belt, Zagros Mountains. Journal of the Geological Society of London, 158, 969-981.

Huber, H., 1977, Tectonic map of Iran (South-East, North-East, North-West,), scale 1:2,500,000. National Iranian Oil Company.

Jackson, J., Haines, A.J., Holt, W.E., 1995. The accommodation of Arabia-Eurasia plate convergence in Iran. Journal of Geophysical Research 100, 15205-15209.

Johnson and Rutherford, 1989. Experimental calibration of the aluminium-inhornblende geobarometer with application to Long Valley Caldeira (California) volcanic rocks. Geology 17, 837-841.

Jung, D., Kursten, M., and Tarkian, M., 1976. Post-Mesozoic volcanism in Iran and its relation to the subduction of the Afro-Arabian under the Eurasian plate. In: Pilger, A., Rosler, A. (Eds.), A far between continental and oceanic rifting. Schweizerbartsche Verlagbuchhandlung, Stuttgart, 175-181.

Kheirkhah, M., Allen, M.B., Emami, M., 2009. Quaternary syn-collision magmatism from the Iran/Turkey borderlands. Journal of Volcanology and Geothermal Research 182, 1-12.

Koop, W.J., and Stoneley, R., 1982. Subsidence history of the Middle East Zagros Basin: Permian to Recent. Philosophical Transactions of the Royal Society of London, Series A: Mathematical and Physical Sciences 305, 149-168.

Leake, B.E., Wooley, A.R., Arps, C.E.S., Birch, W.D., Gilbert, M.C., Grice, J.D., Hawthorne, F.C., Kato, A., Kisch, H.J., Krivovichev, V.G., Linthout, K., Laird, J., Mandarino, J., Maresch, W.V., Nickel, E.H., Rock, N.M.S., Schumacher, J.C., Smith, D.C., Stephenson, N.C.N., Ungaretti, L., Whittaker, E.J.W., Youzhi, G., 1997. Nomenclature of amphiboles: report of the subcommittee on amphiboles of the international mineralogical association commission on new minerals and mineral names. Mineralogical Magazine 61, 295-321.

L'Heureux, I., Fowler, A.D., 1996. Dynamical model of oscillatory zoning in plagioclase with nonlinear partition relation. Geophysical Research Letters 23, 17-20.

Liotard, J.M., *et al.*, 2008. Origin of the absarokite-banakite association of the Damavand volcano (Iran): trace elements and Sr, Nd, Pb isotope constraints. International Journal of Earth Sciences 97, 89-102.

Macdonald, R., Hawkesworth, C.J., Heath, E., 2000. The Lesser Antilles volcanic chain: a study in arc magmatism. Earth-Science Reviews 49, 1-76.

McQuarrie, N., Stock, J.M., Verdel, C., and Wernicke, B.P., 2003. Cenozoic evolution of Neotethys and implications for the causes of plate motions. Geophysical Research Letters, 30, 20, 2036, 6.1-6.6.

Mohajjel M, Fergusson CL, and Sahandi M.R., 2003. Cretaceous-Tertiary convergence and continental collision Sanandaj-Sirjan zone Western Iran. Journal of Asian Earth Science, 21, 397-412.

Moinvazire, H., 1998. An Introduction to Magmatism of Iran. Tehran University Press, Tehran.

Nadimi, A., 2002. Mantle flow patterns at the Neyriz paleospreading center, Iran. Earth and Planetary Science Letters, 203, 93-104.

Nazari, M., Yaghoubpour, A.M., and Madani, H., 1994. Dorreh Kashan barite deposit. Proceedings of Fourth Mining Symposium of Iran, Yazd University, Exploration I, 106-123.

Nicholson, K.N., Khan, M., Mahmood, K., 2010. Geochemistry of the Chagai-Raskoh Arc, Pakistan: Complex arc dynamics spanning the Cretaceous to the Quaternary. Lithos 118 (3-4), 338-348.

Omrani, J., Agard, P., Whitechurch, H., Benoit, M., Prouteau, G., Jolivet, L., 2008. Arc-magmatism and subduction history beneath the Zagros Mountains, Iran: A new report of adakites and geodynamic consequences. Lithos 106, 380-398.

Pearce, J.A., *et al.*, 1990. Genesis of collision volcanism in eastern Anatolia, Turkey. Journal of Volcanology and Geothermal Research 44, 189-229.

Ricou, L.E., 1971. Le croissant ophiolitique péri-arabe, une ceinture de nappes mise en place au crétacé supérieur. Revue de géographie physique et de géologie dynamique, 13, 327-350.

Ricou, L.E., Braud, J. and Brunn, J.H., 1977. Le Zagros, Mem. h.ser. Society of Geology, France, 8, 33-52.

Sabzehei, M., 1994. Geological Quadrangle Map of Iran, No. 12, Hajiabad, 1:250 000, First compilation by Berberian, M. and Final compilation and revision by Sabzehei, M., Geological Survey of Iran.

Saadat, S., 2010. Petrogenesis of Neogene basaltic volcanism associated with the Lut block, eastern Iran: implication for tectonic and metallogenic evolution. Ph.D. Thesis, University of Colorado, Boulder, USA.

Saadat, S., Karimpour, M.H., Stern, C., 2010. Petrochemical characteristics of Neogene and Quaternary alkali olivine basalts from the western margin of the Lut Block, Eastern Iran. Iranian Journal of Earth Sciences 2, 87-106.

Sahandi, M.R., 2006. Geological Map of Shazand. Geological Survey of Iran.

Salkhi, R., 1997. Volcanology and petrology of Quaternary volcanoes of Gehghan-e Bala region-NW of Bazman. M.Sc. Thesis, Shahid Bahonar University of Kerman, Kerman, Iran.

Scaillet, B., Evans, B.W., 1999. The June, 1991 eruption of Mount Pinatubo. Phase equilibria and preeruption P-T-fO2-H2O conditions of the dacite magma. Journal of Petrology 40, 381-411.

Schmidt, M.W., 1992. Amphibole composition in tonalite as a function of pressure: an experimental calibration of the Al-in-hornblende barometer. Contributions to Mineralogy and Petrology 110, 304-310.

Sengor, A.M.C., 1984. The Cimmeride Orogenic System and the Tectonics of Eurasia. Geological Society of America, Special Paper, 195, 82.

Sengör, A.M.C., 1990. A new model for the Late Paleozoic-Mesozoic tectonic evolution of Iran and implications for Oman. In: Robertson, A.H.F., Searle, M.P., Ries, A.C. (Eds.), The Geology and Tectonics of the Oman region. Geological Society, London, Special Publication, 49, 797-831.

Shahabpour, J., 2007. Island-arc affinity of the Central Iranian volcanic belt. Journal of Asian Earth Sciences, 30, 652-665.

Shahabpour, J., and Kramers, J.D., 1987. Lead isotope data from the Sar Cheshmeh porphyry copper deposit, Kerman, Iran. Mineral Deposita, 22, 278-281.

Sheikholeslami, R., Bellon, H., Emami, H., Sabzehei, M., Pique, A., 2003. Nouvelles données structurales et datations 40 K-40Ar sur les roches métamorphiques de la région de Neyriz (zone de Sanandaj - Sirjan, Iran méridional). Leur intérêt dans le cadre du domaine Néo-t éthysien du Moyen-Orient: new structural and 40 K-40Ar data for the metamorphic rocks in Neyriz area (Sanandaj-Sirjan Zone, Southern Iran). Their interest for an overview of the Neo-Tethyan domain in the Middle East. Comptes Rendus Geosciences 335, 981-991.

Siddiqui, R.H., 2004. S type arc affinities of pyroxene diorite from the Tanki Sills, western Chagai Arc, Balochistan, Pakistan. International Geological Congress 32, 1462.

Siebert, L., Simkin, T., 2002. Volcanoes of the World: an Illustrated Catalog of Holocene Volcanoes and their Eruptions. Smithsonian Institution, Global Volcanism Program, Digital Information Series, GVP-3 http://www.volcano.si.edu/world/.

Sisson, T.W., Grove, T.L., 1993. Experimental investigation of the role of water in calcalkaline differentiation and subduction zone magmatism. Contributions to Mineralogy and Petrology 113, 143-166.

Stampfli, G.M., and Borel, G.D., 2002. A plate tectonic model for the Paleozoic and Mesozoic constrained by dynamic plate boundaries and restored synthetic oceanic isochrones. Earth and Planetary Science Letters 196, 17-33.

Stöcklin, J., 1968. Structural history and tectonics of Iran; a review. American Association of Petroleum Geologists Bulletin, 52, 7, 1229-1258.

Stöcklin, J., 1974. Possible ancient continental margin in Iran. In: Burk, C.A., Drake, C.L. (Eds.), the Geology of Continental Margins. Springer, Berlin, 873-887.

Takin, M., 1972. Iranian geology and continental drift in the Middle East. Nature, 23, 147-150.

Torsvik, T.H., and Cocks, L.R.M., 2013. Gondwana from top to base in space and time. Gondwana Research 24, 999-1030.

Valizadeh, M.M., Cantagrel, J.-M., 1975. Premières données radiométriques (K-Ar et RB-Sr) sur les micas du complexe magmatique du Mont Alvand, près de Hamadan (Iran occidental). Comptes Rendus Académie des Sciences Sc. 281.

Vernant, P., Nilforoushan, F., Hatzfeld, D., Abbassi, M.R., Vigny, C., Masson, F., Nankali, H., Martinod, J., Ashtiani, A., Bayer, R., Tavakoli, F., and Chery, J., 2004. Present-day crustal deformation and plate kinematics in the Middle East constrained by GPS measurements in Iran and northern Oman. Geophysical Journal International, 157, 381-398.

Ziegler, P.A., and Stampfli, G.M., 2001. Late Paleozoic-Early Mesozoic plate boundary reorganization: collapse of the Variscan orogen and opening of Neotethys. In: Cassinis, R. (Ed.), the Continental Permian of the Southern Alps and Sardinia (Italy) Regional Reports and General Correlations, Ed. 25. Annali Museo Civico Science Naturali, Brescia, 17-34.